Response to Referee #3

We thank the reviewer for his/her time and consideration, and for the constructive comments. We are confident that all remarks have been carefully addressed and that the manuscript has been improved accordingly. Our point-by-point response is provided below (text in italics denotes excerpts from the revised manuscript).

Referee's comment 1. This study presents RASPBERRY (Real-time Aerosol Source apportionment using Physics-Based Experimental data and multivaRiate factoR analYsis), a novel PM10 source apportionment framework that integrates particle size distributions and spectrally resolved light absorption into a unified Physical PMF (Positive Matrix Factorization). Applied to a five-year hourly dataset (2020–2024) from an urban background site in the Italian Alps, the method successfully identifies six aerosol source factors and demonstrates strong agreement with traditional chemical source apportionment techniques, ground-based remote sensing, and atmospheric modeling tools. RASPBERRY addresses a critical gap in air quality monitoring: the ability to perform high temporal resolution, real-time, continuous, and cost-effective aerosol source apportionment that is based on measurements of aerosol physical properties. The paper is well written and methodologically sound. The 5-year dataset provides excellent statistical robustness and seasonal coverage. The bootstrapping approach for uncertainty estimation reflects best practices in PMF analysis. Validation with chemical PMF, lidar, AERONET AOD, and CAMS reanalysis are thorough. Overall, this paper represents a meaningful and timely contribution to the aerosol science and air quality communities. There are several minor issues: Comment 1: In line 309, the impact of the selected coefficient A, α, and C_3 are not mentioned. Also it is mentioned that "no other modeling uncertainty was included". But other uncertainty sources are not mentioned here but instead was in discussion. So it should be briefly explained to guide the audience to discussion about the rest of the uncertainties.

Author's response 1. We thank the reviewer for the positive overall assessment and for highlighting the limited level of detail originally provided to describe the impact of the uncertainty parameters. Indeed, RASPBERRY reproductivity is actually a goal of this work. To address this potential shortcoming, while at the same time keeping the main text concise, we expanded Sect. S7 of the Supplement. In particular, we now provide a complete description of the procedure used to determine the optimal uncertainty configuration, including the impact of the selected coefficients A, α, and C_3. This workflow is presented in an objective and reproducible manner.

The revised text reads:

The uncertainty framework employed in this study follows the methodology outlined by Vörösmarty et al. (2024), in which the PMF input uncertainty is parametrised as in Eqs. (4) and (5) of the main text. This formulation essentially represents a semi-empirical error model, with notation likely inherited from earlier PMF implementations (PMF2), and separates the uncertainty into two components representing common

sources of uncertainty in aerosol measurements: (i) baseline instrument/analysis noise, ensuring a minimum uncertainty even when concentrations are small; and (ii) a concentration-dependent error, which increases proportionally with the measured concentration. The interested reader is referred to that work, and the references therein, for further details. Here we instead present an objective and reproducible workflow describing, step by step, how the free coefficients A, α, and C_3 were selected:

1. *Choice for A and α started from relevant ranges suggested in the aforementioned study and in the scientific literature (e.g., Zhou et al., 2005a; Ogulei et al., 2006, 2007; Gu et al., 2011), i.e. 0.01 to 0.05 for the product $A \times \alpha$. In our case, $A = 1$ was assigned to size channels and optical absorption, and $\alpha = 0.01$ was used as an initial value, following Vörösmarty et al. (2024).*

2. *Choice for C_3 started from values between 0.01 and 0.5. For example, Vörösmarty et al. (2024) select 0.10 for most of their channels. A value of 10 % represents a reasonable a priori estimate of the uncertainty when no additional information is available, therefore C_3 was initially set to this value in our case.*

3. *We then ensured that the total variable (e.g., PM_{10}) did not influence the factorisation by setting it as 'weak' in the PMF (or by assigning $A = 3$ and $C_3' = C_3 \times 3$).*

4. *An initial PMF run was performed, and the residual distribution (Q/Q_{exp}) for each 'species' (VSD channels from OPC and aethalometer spectral absorption at the measured wavelengths) was recorded. At this stage, the volume distribution component typically dominated the profile splitting and was better reproduced by the PMF, with the exception of the largest size ranges (as also reported by Vörösmarty et al., 2024), whereas spectral absorption contributed only marginally to the separation and was not well reproduced (resulting in a high Q/Q_{exp} ratio). This behaviour arises from the larger number of 'channels' associated with particle size (OPC measurements) compared with those related to multispectral optical absorption (aethalometer). This imbalance was corrected in the subsequent steps.*

5. *We gradually adjusted the uncertainty until three criteria were simultaneously satisfied: (i) the factor contributions remained as uncorrelated as possible; (ii) the scaled residuals fell within the expected range (± 3, Norris et al., 2014); and (iii) the resulting profiles and contributions were physically plausible.*

6. *In our case, reducing the residuals (and the Q/Q_{exp} ratio) for the largest size channels without artificially splitting the coarse 'local resuspension' factor into two modes required increasing their uncertainty. This resulted in $C_3 = 0.3$ for size channels with particles larger than $2\,\mu m$ and $C_3 = 0.4$ for particles above $6\,\mu m$. The $2\,\mu m$ and $6\,\mu m$ thresholds were selected as representative of the desert dust and coarse resuspension modes, based on previous literature (see main text) and the examination of the temporal evolution of the volume size distributions. Indeed, these C_3 values improved the separation between desert dust and local resuspension contributions. Larger uncertainty values tended to merge these contributions, whereas smaller values tended to split the local resuspension factor into multiple modes.*

7. *Conversely, in order for the absorption measurements to contribute effectively to shaping the factor profiles, their uncertainty had to be reduced. In this study, C_3 was set to 0.05 for aethalometer measurements. Using higher values caused the size-related portion of the PMF to dominate due to the larger number of size classes, leading to additional size modes lacking clear physical interpretation. In some configurations, the contributions associated with traffic emissions and residential biomass burning became unrealistically small. Similar issues concerning the mass of the traffic factor were reported by Forello et al. (2023). Notably, the selected configuration yielded PM_{10} contributions for traffic and biomass burning that are consistent with the method described by Aujay-Plouzeau (2020), which is based solely on aethalometer measurements.*

8. *During this process, it was necessary to increase the number of factors relative to the initial run, which was based only on size, in order to accommodate factors emerging from the multispectral absorption-driven splitting (e.g., traffic, biomass burning, condensation-mode secondary aerosols). More details on the selection of the optimal number of factors are provided in Sect. S11.*

9. *The plot of the original and reconstructed time series were examined for each input species to verify whether the selected uncertainty configuration reproduced the original data satisfactorily.*

10. *Note that α primarily affects the PMF behaviour at low concentrations of a species, whereas C_3 influences the behaviour at medium to high concentrations. This distinction is particularly important for species exhibiting a marked seasonal cycle, such as those related to biomass burning. In such cases, the minimum uncertainty (constant component, see Table S1) should be chosen so that winter and summer conditions are clearly distinguished, i.e. situations in which the species is present or absent in the atmosphere are well separated.*

11. *The factor uncertainties were finely adjusted at the end of the procedure by scaling them so that the residuals fell within the expected range of* ±3*. In this study, an additional 20 % increase in all C_3 values was required. The coefficients were scaled accordingly rather than introducing an additional parameter ('Additional model uncertainty') in EPA PMF 5.0. The C_3 values reported in Table S1 include this factor and their reported digits are approximated to* ±0.05 *for clarity.*

The final values for the parameters A, α, and C_3 are shown in Table S1. [...]

It may be noted that:

- *The uncertainty assigned to the largest size channels ($d > 6\,\mu m$) is relatively high. This reflects the low number concentration of large particles and their 'shot' nature, which introduces greater variability when considered from a Poisson-based perspective (Sect. S2.1). Indeed, these bins typically contain a few peak values emerging from a background of zeros, whose frequency can reach up to 30 %. Consequently, these size channels, together with the total variable PM_{10}, were classified as weak variables in the PMF configuration to prevent them from exerting excessive influence during subsequent tests. During the testing phase, as suggested in previous studies (e.g., Zhou et al., 2004; Thimmaiah et al., 2009; Zhou et al., 2005b), an alternative approach was also evaluated in which the largest size bins were grouped (in sets of three to five, depending on particle size) to mitigate issues associated with low particle counts and to improve the signal-to-noise ratio (SNR). Although bin grouping effectively increased the SNR, it hindered the separation of the two coarse factors (desert dust and local resuspension). For this reason, this approach was not adopted in the final configuration.*

- *The NeBC uncertainties used in this study are lower than those reported in some previous works (e.g., Forello et al., 2019; Rigler et al., 2020). In particular, Forello et al. (2023) applied an uncertainty as high as 50 % for b_{abs} to avoid convergence issues when coupling absorption data with chemical data in the PMF. With such high uncertainty values, combined with the smaller number of optical variables relative to chemical species, the NeBC information effectively follows the factorisation rather than contributing to it. In contrast, the present approach aims to ensure that both spectral absorption and volume size distribution contribute to determining the final solution. Consequently, the uncertainty values adopted here should not be interpreted as strict measurement uncertainties, but rather as weighting parameters used to balance the influence of the different input variables on the Q metric.*

The sentence "no other modelling uncertainty was included" refers to the field Extra Modelling Uncertainty (%) (EMU) available in one of the configuration windows of the EPA PMF software. This parameter allows the user to artificially increase the declared uncertainty of the input data. In the present study, this parameter was not used because the input uncertainties had already been appropriately defined within the uncertainty framework described in Sect. 3.2.1. The sentence has therefore been clarified as follows: *The field Extra Modelling Uncertainty of the EPA PMF was left unchanged (0%).*

In addition, taking the suggestions received in the review process into account, the manuscript has been expanded by including the application of the Effective Variance Least Squares (EVLS) method to RASPBERRY. This method allows the measurement uncertainties of the input data to be fully propagated to the retrievals, together with the uncertainty associated with rotational ambiguity in the profiles. The method is now illustrated and discussed in the revised manuscript.

A clarifying sentence has also been added to Sect. 3.1.2 based on the reviewer's suggestion to anticipate the discussion: *These values refer to the input uncertainties used in the training (PMF) phase of RASPBERRY. A more comprehensive overview of the method limitations and of the overall uncertainties associated with the retrievals is provided in Sects. 3.3 and 5.*

RC2. In line 330, the seasonal balanced sample selection is mentioned, if the samples are not daily, is the diurnal sampling also balanced?

AR2. We thank the reviewer for this comment, and it is true that this detail was not explicitly stated in the original manuscript. This information has now been added to the revised manuscript, Sect. 3.2: *Owing to the continuous 24 h measurement coverage in the original dataset, the random sampling procedure also results in a nearly homogeneous distribution of observations throughout the day. For example, when considering four day-quarter intervals (0–6, 6–12, 12–18, and 18–24 h), the maximum deviation from a uniform distribution is approximately 3 %.*

This is illustrated in Fig. 1 in this document for the reviewer's reference.

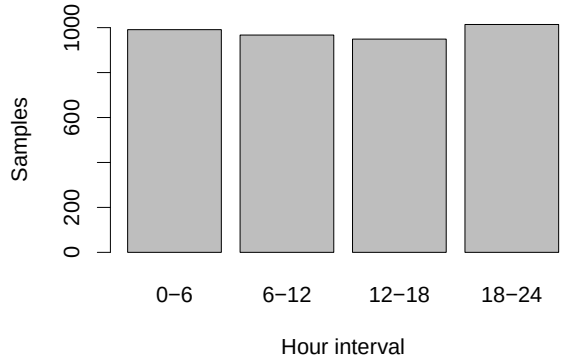

Figure 1: Frequency distribution of samples used for RASPBERRY training across day quarters.

RC3. Line 610, the pink means dust touching the ground in Figs. S24 or in Figure 7? Also is there any lidar to proof that the differences between AERONET and RASPBERRY are due to aloft and surface dust?

AR3. The sentence was modified as follows to avoid confusion (note that the colour description has now been changed to 'yellow', according to a comment by referee #2): *Furthermore, based on the analysis of vertical profiles from the ALCs in Aosta–Saint-Christophe, dust layers that remain primarily aloft (light blue bands in Fig. 7b), detected by the sun photometer but not by the in-situ surface instruments, are discriminated from those that ultimately enter the mixing layer and reach the ground (yellow bands in Fig. 7b). Representative examples are shown using lidar diagrams in Figs. S31a–S31d.*

Co-located automated lidar-ceilometers (ALCs) were indeed used to attribute the observed differences between AERONET and RASPBERRY to dust layers remaining aloft or reaching the surface. The cases

illustrated by the blue and yellow bands were manually verified using the corresponding lidar profiles in order to ensure the robustness of the classification.

RC4. Figure 8a, the differences between chem-PMFd1 and RASPBERRY is very hard to tell due to similar colors. For Fig. 8b, the liner regression cannot represent the true trend of this data. What causes the large scattering in traffic emission contribution? For Secondary rich factors, high bias can be seen throughout, what is the main cause?

AR4. The colours in Fig. 8a were further contrasted to improve readability and facilitate the distinction between chem-PMFd1 and RASPBERRY. The updated plot is reported here as Fig. 2.

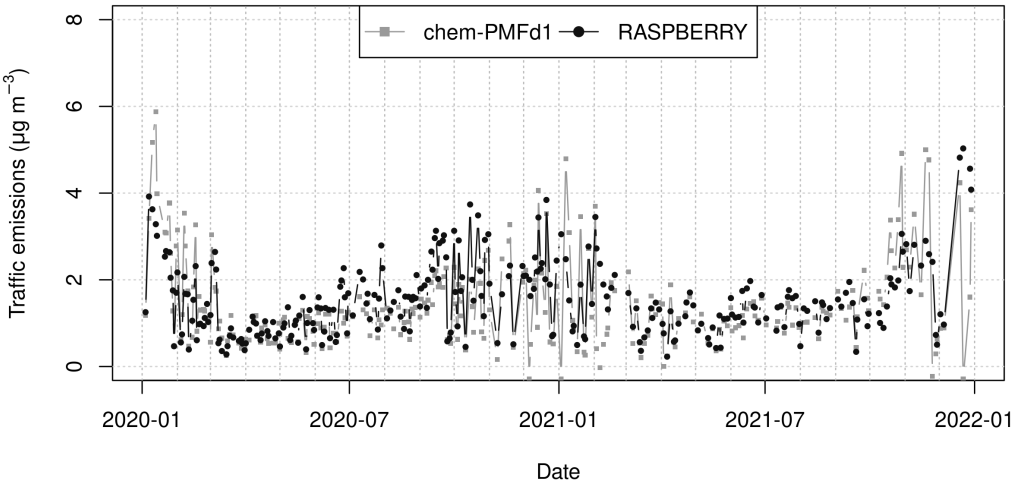

Figure 2: Comparison of daily averaged PM_{10} contribution attributed to traffic derived from the chemical PMF and RASPBERRY.

Regarding the traffic factor, and notably the scattering and the apparent inadequacy of the linear regression, the inclusion of the EVLS method in the revised manuscript provides additional insight into the imperfect agreement between the physical and chemical source apportionment for this source. Indeed, as Aosta is not a large and heavily trafficked city (33,000 inhabitants; Diémoz et al., 2019, 2021), the contributions derived from both the physical and chemical approaches are relatively small and consistently remain below a few $\mu g\,m^{-3}$. At the same time, the relative uncertainty associated with traffic emissions is among the highest of all dimensional profiles. This combination of low signal and comparatively large uncertainty naturally leads to a substantial dispersion in the point-to-point comparison (Fig. 3, complementing the results in Fig. 8b reported in the first version of the manuscript and now included in Fig. S34).

The corresponding paragraph in Sect. 4.3 was therefore updated as follows:

The comparison of traffic factors is depicted in Figs. 8a (time series) and 8b (scatter plot). From the first panel, it is evident that the magnitude of contributions from both source apportionments is about the same, as are the overall seasonal trends. However, the point-to-point relationship illustrated in the second panel reveals some discrepancies, with a Pearson's correlation coefficient of $\rho = 0.67$ *(*$R^2 = 0.45$*). Furthermore, the regression coefficients deviate from the 1:1 line (*$y = 0.58\,x + 0.72\ \mu g\,m^{-3}$*). This deviation can be attributed to difficulties in accurately identifying the traffic factor, primarily due to the following reasons:*

– *Contributions from both source apportionments are relatively low, steadily remaining below 6* $\mu g\,m^{-3}$*,*

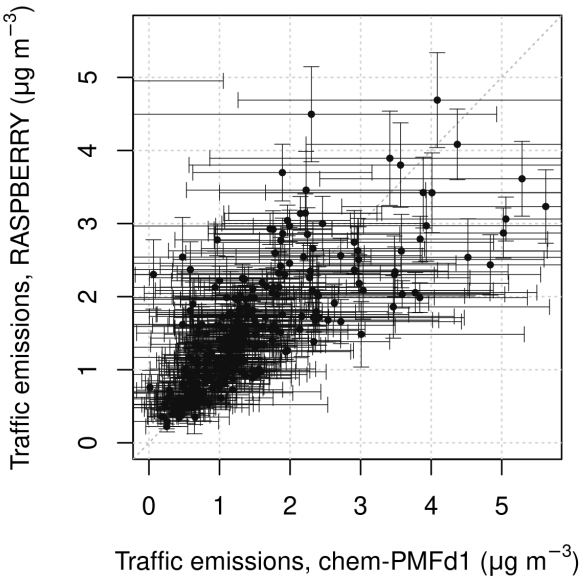

Figure 3: Comparison of daily-averaged PM_{10} source contributions attributed to traffic derived from the chemical PMF (further reprocessed using EVLS) and RASPBERRY+EVLS, shown together with their individual uncertainties. The figure clearly shows that the uncertainty in the chemical source apportionment is larger than in the physical one.

which is consistent with the fact that Aosta is a relatively small, low-traffic city (33,000 inhabitants; Diémoz et al., 2019, 2020, 2021). At the same time, the relative uncertainty associated with traffic emissions is among the highest of all dimensional profiles. This is evident from both the large interval ratio obtained from the DISP test (Sect. 4.2 and Fig. 3) and from the uncertainties derived using the EVLS method for both the physical and the chemical data sets (Fig. S34).

- *The finite lower detection limit of the OPC does not allow all aerosols emitted by traffic to be captured. In particular, most of the studies focusing on ultrafine and accumulation-mode particles (among the most recent examples, Harni et al., 2024; Beddows et al., 2025; Ćirović et al., 2026; Mapelli et al., 2026) identified at least two distinct factors related to traffic (e.g., freshly nucleated vs more aged or distant particles, or gasoline vs diesel/heavy-duty emissions). This may indicate that the physical setup and the chemical analyses effectively 'detect' different factors attributed to traffic.*
- *The coarse resuspended fraction, which significantly contributes to the mass, may be characterised in slightly different amounts in the chemical and the physical source apportionments, as discussed in Sect. S10. Distinguishing unambiguously exhaust and non-exhaust particle contributions is a well-known challenge, frequently reported in the literature (Forello et al., 2023).*
- *The mass absorption cross-section (MAC) in aethalometer measurements may decrease in winter compared to summer, as observed in several studies, e.g. Mousavi et al. (2019) in Milan and Savadkoohi et al. (2024) on a European scale. Such seasonal variation is consistent with an underestimation of NeBC during winter, when concentrations are higher, and an overestimation during summer, when concentrations are lower, in RASPBERRY.*

At the same time, it should be noted that the comparison slope for the traffic factor is higher than 1 when using York and log-transformed York regressions (Table S3), since the intercept decreases. Therefore, the deviation from the 1:1 line may also be partly attributable to an artefact of the regression method itself.

Regarding the secondary-rich factor, the apparent high bias observed in the regression was further analysed to determine whether it represents a systematic data feature or rather depends on the specific regression technique employed. To this end, as already anticipated in the answer above, we recalculated

the regression using several alternative and more advanced approaches, reported in the table below, namely: (i) total least squares (Deming regression; Linnet, 1990), performed by accounting for the actual variance-error ratios obtained from the DISP test of both the physical and chemical PMF solutions; (ii) York regression (York et al., 2004), performed using individual uncertainties calculated through EVLS for both the physical (RASPBERRY+EVLS) and chemical (PMF+EVLS) data sets; and (iii) York regression applied to log-transformed quantities to account for heteroscedasticity in the data.

Table 1: Regression coefficients and their standard errors between the PM_{10} contributions from the chemical PMF (x) and RASPBERRY(+EVLS) (y), determined using different regression methods: ordinary least squares (OLS), Deming regression (total least squares, Linnet, 1990), York regression (York et al., 2004), and log-log York regression to account for heteroscedasticity.

Method	Coefficients	Traffic	Biomass burning	Secondary [a]	Coarse [b]
OLS	Slope	0.58 ± 0.04	0.99 ± 0.02	0.99 ± 0.04	0.95 ± 0.03
	Intercept ($\mu g\,m^{-3}$)	0.72 ± 0.06	0.34 ± 0.04	1.62 ± 0.28	1.36 ± 0.19
Deming [c]	Slope	0.60 ± 0.05	1.08 ± 0.04	1.08 ± 0.05	0.96 ± 0.05
	Intercept ($\mu g\,m^{-3}$)	0.70 ± 0.09	0.22 ± 0.03	1.16 ± 0.24	1.31 ± 0.20
York [d]	Slope	1.35 ± 0.12	1.20 ± 0.03	1.32 ± 0.03	1.58 ± 0.03
	Intercept ($\mu g\,m^{-3}$)	-0.16 ± 0.11	0.12 ± 0.01	0.01 ± 0.12	-0.88 ± 0.08
York (log)	Slope	1.05 ± 0.08	0.86 ± 0.02	1.26 ± 0.04	1.32 ± 0.02
	Intercept ($\mu g\,m^{-3}$)	0.01 ± 0.05	0.32 ± 0.02	-0.51 ± 0.08	-0.41 ± 0.03

[a] Sum of sulfate- and nitrate-rich factors from the chemical PMF, and condensation and droplet mode factors from RASPBERRY.
[b] Sum of road salting and crustal factors from the chemical PMF, and desert dust and local dust resuspension from RASPBERRY, excluding data influenced by significant Saharan dust events.
[c] The regression was performed taking into account the actual variance-error ratios obtained from the DISP test of both physical and chemical PMFs. RASPBERRY retrievals were used with this method.
[d] The regression was performed using individual uncertainties calculated through EVLS for both the physical (RASPBERRY+EVLS) and chemical (PMF+EVLS) data sets (Fig. S34). York et al. (2004) regression yields the same coefficients as those obtained using Python's implementation of orthogonal distance regression (ODR).

The main text was correspondingly updated with the remark: *[...] the large positive intercept for the secondary factors is statistically significant when using OLS and Deming regressions, but not with York regression, and it turns negative (and statistically significant) when York regression is applied to log-transformed data. This result suggests that, similarly to traffic, the apparent high bias is largely an artefact of the regression method, and perhaps of the heteroscedastic nature of the data, rather than a systematic discrepancy between the two source apportionment approaches.*

RC5. Figure 13 e and f, the vertical level where backscattering shows smoke, does not have valid retrieval of depolarization ratio in g and h. (For example, the small chunk of smoke at 5km in 13f, the location is corresponding to noise/no-retrieval for 13h.)

AR5. The reviewer is correct. This limitation has now been clarified in the revised manuscript. Specifically, we state: *It should be noted that aerosol depolarisation measurements obtained with the CL61 generally exhibit low signal-to-noise ratios, particularly for elevated and optically thin layers (Looschelders et al., 2025). Consequently, the smoke layers identified in the backscatter profiles (Figs. 13e–f) cannot be robustly characterised in terms of their depolarisation properties.* The figure caption has also been up-

dated accordingly: *Note that, in this case, the low smoke depolarisation, together with the weak signal-to-noise ratio of the CL61, limits reliable depolarisation measurements to the lowest atmospheric layers.* In addition, we have improved the visualisation by applying a more accurate mask based on the signal-to-noise ratio of the backscatter coefficient, and particle depolarisation ratio is now shown instead of volume depolarisation ratio, ensuring consistency with recent literature.

References

Aujay-Plouzeau, R.: Guide méthodologique pour la mesure du «Black Carbon» par Aethalomètre multi longueur d'onde AE33 dans l'air ambiant (Version 2020), Tech. rep., Ineris, https://www.lcsqa.org/system/files/media/documents/LCSQA2019-Guide_mesure_BlackCarbon_par_AE33_VF03-Approuv%C3%A9CPS15122020.pdf, 2020.

Beddows, D., Brean, J., Rowell, A., Merkel, M., Weinhold, K., Dall'Osto, M., and Harrison, R.: Wide-Positive Matrix Factorisation of particle number size distributions: A new approach accounting for cyclically changing source profiles, Sci. Total Environ., 998, 180 231, https://doi.org/10.1016/j.scitotenv.2025.180231, 2025.

Ćirović, Ž., Stojanović, D. B., Davidović, M., Onjia, A., Alastuey, A., and Jovašević-Stojanović, M.: New Particle Formation and Source Apportionment of Particle Number Size Distribution in the Urban Area of the City of Belgrade, Atmosphere, 17, https://doi.org/10.3390/atmos17020205, 2026.

Diémoz, H., Gobbi, G. P., Magri, T., Pession, G., Pittavino, S., Tombolato, I. K. F., Campanelli, M., and Barnaba, F.: Transport of Po Valley aerosol pollution to the northwestern Alps – Part 2: Long-term impact on air quality, Atmos. Chem. Phys., 19, 10 129–10 160, https://doi.org/10.5194/acp-19-10129-2019, 2019.

Diémoz, H., Tombolato, I. K. F., Zublena, M., Magri, T., and Ferrero, L.: The impact of biomass burning emissions on PM concentration in the Greater Alpine region, in: Proceedings of 12th International Conference on Air Quality, Science and Application, p. 26, Hatfield, UK, 10.18745/pb.22217, 2020.

Diémoz, H., Magri, T., Pession, G., Tarricone, C., Tombolato, I. K. F., Fasano, G., and Zublena, M.: Air Quality in the Italian Northwestern Alps during Year 2020: Assessment of the COVID-19 «Lockdown Effect» from Multi-Technique Observations and Models, Atmosphere, 12, https://doi.org/10.3390/atmos12081006, 2021.

Forello, A. C., Bernardoni, V., Calzolai, G., Lucarelli, F., Massabò, D., Nava, S., Pileci, R. E., Prati, P., Valentini, S., Valli, G., and Vecchi, R.: Exploiting multi-wavelength aerosol absorption coefficients in a multi-time resolution source apportionment study to retrieve source-dependent absorption parameters, Atmos. Chem. Phys., 19, 11 235–11 252, https://doi.org/10.5194/acp-19-11235-2019, 2019.

Forello, A. C., Cunha-Lopes, I., Almeida, S. M., Alves, C. A., Tchepel, O., Crova, F., and Vecchi, R.: Insights on the combination of off-line and on-line measurement approaches for source apportionment studies, Sci. Total Environ., 900, 165 860, https://doi.org/10.1016/j.scitotenv.2023.165860, 2023.

Gu, J., Pitz, M., Schnelle-Kreis, J., Diemer, J., Reller, A., Zimmermann, R., Soentgen, J., Stoelzel, M., Wichmann, H.-E., Peters, A., and Cyrys, J.: Source apportionment of ambient particles: Comparison of positive matrix factorization analysis applied to particle size distribution and chemical composition data, Atmos. Environ., 45, 1849–1857, https://doi.org/10.1016/j.atmosenv.2011.01.009, 2011.

Harni, S. D., Aurela, M., Saarikoski, S., Niemi, J. V., Portin, H., Manninen, H., Leinonen, V., Aalto, P., Hopke, P. K., Petäjä, T., Rönkkö, T., and Timonen, H.: Source apportionment of particle number size distribution at the street canyon and urban background sites, Atmos. Chem. Phys., 24, 12 143–12 160, https://doi.org/10.5194/acp-24-12143-2024, 2024.

Linnet, K.: Estimation of the linear relationship between the measurements of two methods with proportional errors, Stat. Med., 9, 1463–1473, https://doi.org/10.1002/sim.4780091210, 1990.

Looschelders, D., Christen, A., Grimmond, S., Kotthaus, S., Fenner, D., Dupont, J.-C., Haeffelin, M., and Morrison, W.: Inter-Instrument Variability of Vaisala CL61 Lidar-Ceilometer's Attenuated Backscatter, Cloud Properties and Mixed-Layer Height, Meteorol. Appl., 32, e70 088, https://doi.org/10.1002/met.70088, 2025.

Mapelli, C., Diémoz, H., Contini, D., Dinoi, A., Cesari, D., and Barnaba, F.: Physics-based aerosol source apportionment at the site of Lecce (Italy), Atmos. Res. (under review), 2026.

Mousavi, A., Sowlat, M. H., Lovett, C., Rauber, M., Szidat, S., Boffi, R., Borgini, A., De Marco, C., Ruprecht, A. A., and Sioutas, C.: Source apportionment of black carbon (BC) from fossil fuel and biomass burning in metropolitan Milan, Italy, Atmos. Environ., 203, 252–261, https://doi.org/10.1016/j.atmosenv.2019.02.009, 2019.

Norris, G., Duvall, R., and Brown, S.: EPA Positive Matrix Factorization (PMF) 5.0 Fundamentals and User Guide, U.S. Environmental Protection Agency Office of Research and Development Washington, DC 20460, `https://www.epa.gov/sites/default/files/2015-02/documents/pmf_5.0_user_guide.pdf`, ePA/600/R-14/108, 2014.

Ogulei, D., Hopke, P. K., Zhou, L., Pancras, J. P., Nair, N., and Ondov, J. M.: Source apportionment of Baltimore aerosol from combined size distribution and chemical composition data, Atmos. Environ., 40, 396–410, https://doi.org/10.1016/j.atmosenv.2005.11.075, 2006.

Ogulei, D., Hopke, P. K., Chalupa, D. C., , and Utell, M. J.: Modeling Source Contributions to Submicron Particle Number Concentrations Measured in Rochester, New York, Aerosol Sci. Tech., 41, 179–201, https://doi.org/10.1080/02786820601116012, 2007.

Rigler, M., Drinovec, L., Lavrič, G., Vlachou, A., Prévôt, A. S. H., Jaffrezo, J. L., Stavroulas, I., Sciare, J., Burger, J., Kranjc, I., Turšič, J., Hansen, A. D. A., and Močnik, G.: The new instrument using a TC–BC (total carbon–black carbon) method for the online measurement of carbonaceous aerosols, Atmos. Meas. Tech., 13, 4333–4351, https://doi.org/10.5194/amt-13-4333-2020, 2020.

Savadkoohi, M., Pandolfi, M., Favez, O., Putaud, J.-P., Eleftheriadis, K., Fiebig, M., Hopke, P. K., Laj, P., Wiedensohler, A., Alados-Arboledas, L., Bastian, S., Chazeau, B., Álvaro Clemente María, Colombi, C., Costabile, F., Green, D. C., Hueglin, C., Liakakou, E., Luoma, K., Listrani, S., Mihalopoulos, N., Marchand, N., Močnik, G., Niemi, J. V., Ondráček, J., Petit, J.-E., Rattigan, O. V., Reche, C., Timonen, H., Titos, G., Tremper, A. H., Vratolis, S., Vodička, P., Funes, E. Y., Zíková, N., Harrison, R. M., Petäjä, T., Alastuey, A., and Querol, X.: Recommendations for reporting equivalent black carbon (eBC) mass concentrations based on long-term pan-European in-situ observations, Environ. Int., 185, 108 553, https://doi.org/10.1016/j.envint.2024.108553, 2024.

Thimmaiah, D., Hovorka, J., and Hopke, P. K.: Source apportionment of winter submicron prague aerosols from combined particle number size distribution and gaseous composition data, Aerosol Air Qual. Res., 9, 209–236, https://doi.org/10.4209/aaqr.2008.11.0055, 2009.

Vörösmarty, M., Hopke, P. K., and Salma, I.: Attribution of aerosol particle number size distributions to main sources using an 11-year urban dataset, Atmos. Chem. Phys., 24, 5695–5712, https://doi.org/10.5194/acp-24-5695-2024, 2024.

York, D., Evensen, N. M., Martínez, M. L., and De Basabe Delgado, J.: Unified equations for the slope, intercept, and standard errors of the best straight line, Am. J. Phys., 72, 367–375, https://doi.org/10.1119/1.1632486, 2004.

Zhou, L., Hopke, P. K., Paatero, P., Ondov, J. M., Pancras, J., Pekney, N. J., and Davidson, C. I.: Advanced factor analysis for multiple time resolution aerosol composition data, Atmos. Environ., 38, 4909–4920, https://doi.org/10.1016/j.atmosenv.2004.05.040, 2004.

Zhou, L., Hopke, P. K., Stanier, C. O., Pandis, S. N., Ondov, J. M., and Pancras, J. P.: Investigation of the relationship between chemical composition and size distribution of airborne particles by partial least squares and positive matrix factorization, J. Geophys. Res., 110, https://doi.org/10.1029/2004JD005050, 2005a.

Zhou, L., Kim, E., Hopke, P. K., Stanier, C., and Pandis, S. N.: Mining airborne particulate size distribution data by positive matrix factorization, J. Geophys. Res., 110, https://doi.org/10.1029/2004JD004707, 2005b.